Effect of the interfacial continuity on the elastic full-waveform inversion

Ourania Giannopoulou

Independent Researcher, Rome, Italy

Department of Engineering, Tor Vergata University of Rome, Italy (former affiliation)

ORCID: 0000-0002-0773-2939

urania.giannopoulou@gmail.com

This is a non peer-reviewed preprint submitted to EarthArXiv.

A version of this work has been submitted to the journal *Geophysical Journal International* for peer review.

Effect of the interfacial continuity on the elastic full-waveform inversion

Ourania Giannopoulou
Independent Researcher, Rome, Italy
Department of Engineering, Tor Vergata University of Rome, Italy (former affiliation)
ORCID: 0000-0002-0773-2939
urania.giannopoulou@gmail.com

Preprint. This is a non peer-reviewed Author's Original Version submitted to EarthArXiv. A version of this work has been submitted to *Geophysical Journal International.*

Abstract

Full-waveform inversion (FWI) routinely assumes welded interfaces between subsurface layers, yet many geological and engineering targets — including karst cavities, fractures, and unbonded soil-structure contacts — exhibit interfacial slip. We show that this modelling assumption is not merely a geometric detail but introduces a systematic bias in the recovered physical parameters. Using a finite-element full-waveform-inversion (FWI) framework implemented in FEniCS, we compare two interfacial treatments: a standard continuous Galerkin (CG) formulation that enforces welded continuity, and a discontinuous Galerkin (DG) formulation based on Nitsche's method that permits tangential slip at material boundaries. A synthetic "inversion crime" cross-test on a two-dimensional elastic inclusion model demonstrates that the CG solver absorbs the interfacial slip effects through biased density estimates, achieving a numerically lower misfit at the cost of parameter accuracy. The DG formulation, by contrast, maintains physical consistency and recovers more accurate parameter values. Our results highlight the need for practitioners to carefully consider interfacial continuity assumptions when inverting seismic data from environments where welded boundary conditions may not hold.

Key words: waveform inversion; numerical modelling; elasticity and anelasticity; computational seismology; wave propagation; inverse theory

1 Introduction

Full-waveform inversion (FWI) leverages the complete seismic waveform to reconstruct subsurface elastic parameters and has become a cornerstone technique in exploration geophysics and seismology (Virieux, 1986; Tarantola, 1984). Over the past four decades, FWI has evolved from acoustic single-parameter inversion to multi-parameter elastic formulations capable of recovering density, P-wave velocity, and S-wave velocity simultaneously (Virieux & Operto, 2009; Operto et al., 2013). Despite these advances, the vast majority of elastic FWI implementations assume that adjacent subsurface layers satisfy a *welded* interface condition— meaning both displacement and traction are continuous across the boundary.

However, numerous geological and engineering targets of practical interest violate this assumption. Karst cavities, buried voids, masonry–soil contacts, fracture networks, and poorly consolidated stratigraphic boundaries can all exhibit tangential slip, partial debonding, or frictional sliding (Signorini, 1940; Mavko et al., 2009). When the observed wavefield carries signatures of such interfacial processes, an FWI solver that enforces welded boundary conditions attributes the slip-induced wavefield modifications to bulk elastic parameters, producing systematic bias in the recovered density and stiffness estimates.

The Discontinuous Galerkin (DG) method naturally accommodates displacement discontinuities across element interfaces through numerical flux terms and penalty parameters (Arnold et al., 2002; Hansbo & Hansbo, 2002). In particular, Nitsche's interior penalty formulation enforces interface constraints weakly in a variationally consistent manner while permitting tangential slip (Nitsche, 1971). Although DG methods have been widely adopted for seismic forward modelling (Ainsworth, 2006; Fezoui & Christon, 2005), their systematic integration into elastic FWI inversion workflows—where the forward operator, sensitivity computation, and optimisation loop must remain strictly consistent—remains an open research question.

In this study, we investigate the effect of interfacial continuity assumptions on elastic FWI parameter accuracy. We implement both CG and DG forward solvers within the open-source finite-element platform FEniCS (Logg et al., 2012) and design a systematic cross-test on a two-dimensional elastic inclusion model. Synthetic data are generated with the DG solver, which captures interfacial slip physics, and subsequently inverted by both the CG and DG solvers. Our results demonstrate that the CG solver cannot represent the interfacial slip mechanism and compensates by biasing the density estimate upward, whereas the DG solver maintains physical consistency and recovers more accurate parameter values.

2 Methodology

2.1 Model setup

Consider a two-dimensional elastic domain Ω containing a circular inclusion (the "cavity") embedded in a homogeneous background medium. The true inclusion has density $\rho_o = 7.0$ and Lamé parameters $\mu_o = 2.0$, $\lambda_o = 4.0$ (in normalised units), while the background has $\rho_b = 3.5$, $\mu_b = 1.0$, $\lambda_b = 2.0$. A seismic source is excited at the surface and the wavefield is recorded by a receiver array (Fig. 1).

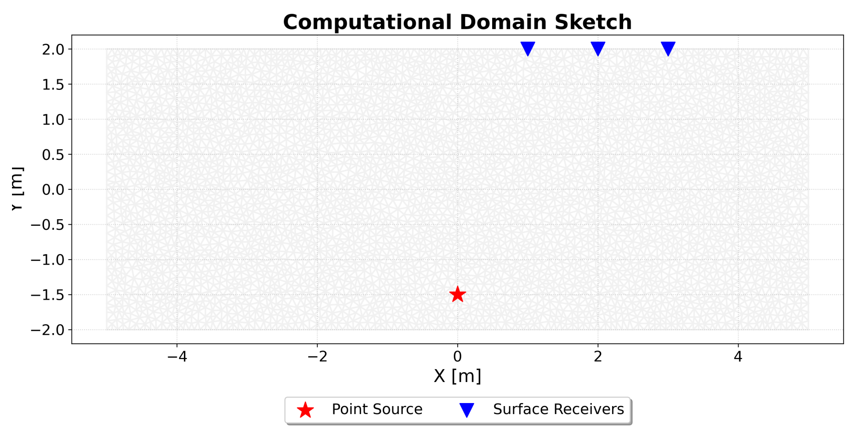

Figure 1: Computational domain showing the seismic source, receiver array, and target inclusion embedded in a homogeneous background.

2.2 Forward modelling

Wave propagation is governed by the 2D elastodynamic equation:

$$\rho \frac{\partial^2 \mathbf{u}}{\partial t^2} - \nabla \cdot \boldsymbol{\sigma}(\mathbf{u}) = \mathbf{f}, \tag{1}$$

where $\mathbf{u}$ is the displacement vector, $\boldsymbol{\sigma}$ is the stress tensor, and $\mathbf{f}$ the source term. The constitutive relation reads:

$$\boldsymbol{\sigma} = \lambda(\nabla \cdot \mathbf{u})\mathbf{I} + 2\mu\, \boldsymbol{\varepsilon}(\mathbf{u}), \tag{2}$$

with $\boldsymbol{\varepsilon} = \frac{1}{2}(\nabla \mathbf{u} + \nabla \mathbf{u}^T)$ the strain tensor.

2.2.1 Continuous Galerkin (CG) formulation

In the standard CG formulation, the displacement field is approximated in the continuous finite-element space $V_h = \{v \in H^1(\Omega) : v|_T \in \mathcal{P}_1(T)\}$. The weak form reads:

$$\int_\Omega \rho \frac{\partial^2 \mathbf{u}}{\partial t^2} \cdot \mathbf{v}\, dx + \int_\Omega \boldsymbol{\sigma}(\mathbf{u}) : \boldsymbol{\varepsilon}(\mathbf{v})\, dx = \int_\Omega \mathbf{f} \cdot \mathbf{v}\, dx, \tag{3}$$

for all test functions $\mathbf{v} \in V_h$. The C^0 continuity of the trial space enforces displacement continuity across element boundaries and hence welded contact at the inclusion interface.

2.2.2 Discontinuous Galerkin (DG) formulation with Nitsche's method

In the DG formulation, the displacement is approximated in the broken finite-element space that allows discontinuities across element boundaries. Nitsche's interior penalty method (Nitsche, 1971; Arnold et al., 2002) weakly enforces interface conditions through additional surface integrals on the inclusion boundary dS:

$$\int_\Omega \rho \frac{\partial^2 \mathbf{u}}{\partial t^2} \cdot \mathbf{v}\, dx + \int_\Omega \boldsymbol{\sigma}(\mathbf{u}) : \boldsymbol{\varepsilon}(\mathbf{v})\, dx + J_{\text{pen}}(\mathbf{u}, \mathbf{v}) = \int_\Omega \mathbf{f} \cdot \mathbf{v}\, dx, \tag{4}$$

where the penalty term J_{pen} preserves normal continuity while permitting tangential slip:

$$J_{\text{pen}} = \int_{dS} \left(\sigma_n [\![\mathbf{u}]\!] \cdot [\![\mathbf{v}]\!] + \sigma_t(\mathbf{u}) \cdot [\![\mathbf{v}]\!]_t + \gamma [\![\mathbf{u}]\!] \cdot [\![\mathbf{v}]\!]\right) dS, \tag{5}$$

with $[\![\cdot]\!]$ the jump across the interface, σ_n and σ_t the normal and tangential stress components, and $\gamma > 0$ the penalty parameter. The key feature of the DG formulation is that no constraint is imposed on tangential displacement continuity, thereby allowing physically meaningful slip at the inclusion boundary.

2.3 Inversion framework

The FWI objective function is the L_2 data misfit between observed and predicted seismograms:

$$J(\mathbf{m}) = \frac{1}{2} \sum_{r=1}^{N_r} \int_0^T |u_{\text{pred}}(\mathbf{x}_r, t; \mathbf{m}) - u_{\text{obs}}(\mathbf{x}_r, t)|^2\, dt, \tag{6}$$

where $\mathbf{m} = \{\rho, \mu, \lambda\}$ is the parameter vector and the sum runs over all N_r receiver locations $\mathbf{x}_r$.

Gradient-based optimisation uses parameter-wise gradients approximated via central finite differences:

$$\frac{\partial J}{\partial m_i} \approx \frac{J(m_i + \Delta m_i) - J(m_i - \Delta m_i)}{2\Delta m_i}. \tag{7}$$

This adjoint-free approach avoids the derivation of adjoint operators for each parameter, at the cost of $2N_m$ forward solves per iteration (N_m being the number of parameters). For the small-scale models considered here, this trade-off is acceptable.

3 The "inversion crime" cross-test

To isolate the effect of interfacial continuity assumptions, we design a synthetic cross-test in which the *observed data are generated with the DG solver* (including interfacial slip effects). The data are subsequently inverted by both solvers:

1. **CG solver (welded):** Assumes displacement continuity at the inclusion interface. This constitutes the "inversion crime" — using a physically inconsistent forward operator.
2. **DG solver (non-welded):** Consistent with the data-generating physics. The "correct" inversion.

Both solvers use identical initial models ($\rho_0 = 3.5$, $\mu_0 = 1.0$, $\lambda_0 = 2.0$), optimisation parameters (learning rate = 0.5, central FD step sizes $\Delta\rho = 0.1$, $\Delta\mu = 0.05$, $\Delta\lambda = 0.1$), and convergence criteria. The comparison isolates the forward-operator discretisation as the sole variable.

4 Results

4.1 Wavefield differences between CG and DG

Figure 2 compares elastic wavefield snapshots produced by the CG and DG solvers for identical source and material parameters. Both exhibit similar large-scale propagation patterns, yet the DG wavefield shows additional diffraction signatures emanating from the inclusion interface, consistent with interfacial slip and mode conversion.

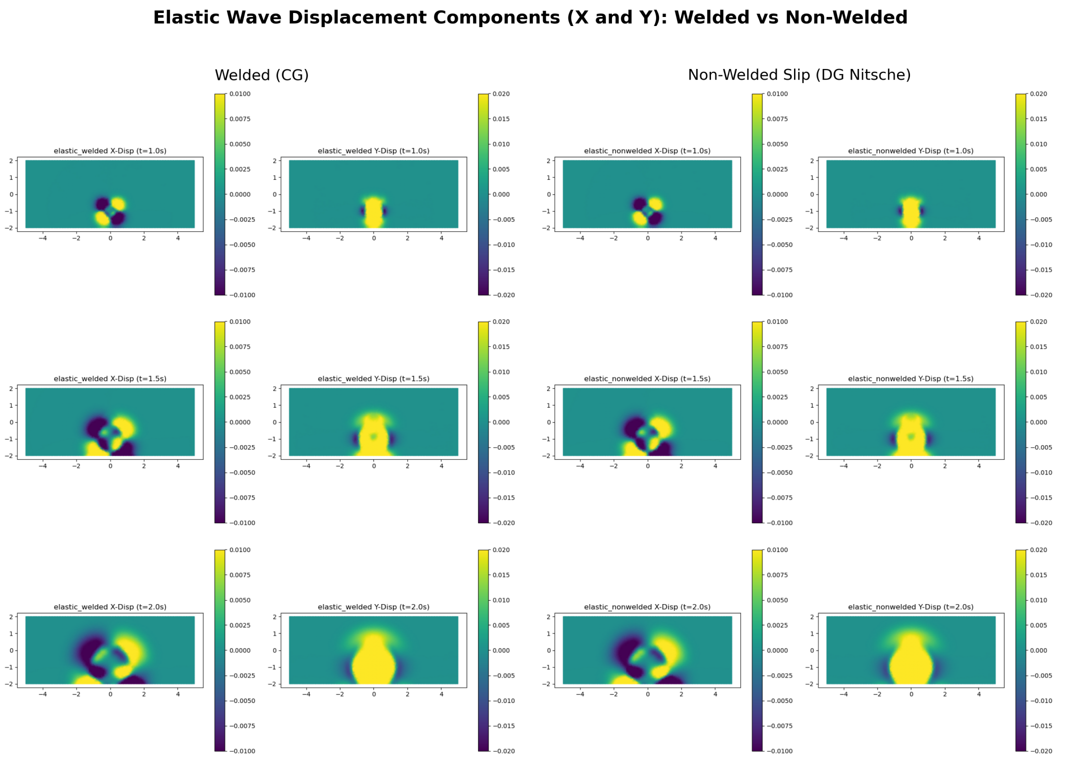

Figure 2: Elastic wavefield snapshots: CG (welded, left) and DG (non-welded, right). The DG wavefield exhibits additional diffraction generated by interfacial slip at the inclusion boundary.

The spatial distribution of the difference $|u_{\text{DG}} - u_{\text{CG}}|$ (Fig. 3) confirms that the discrepancy is concentrated at the inclusion boundary and propagates outward as a secondary wavefield, demonstrating that the interfacial treatment fundamentally alters the wavefield throughout the domain.

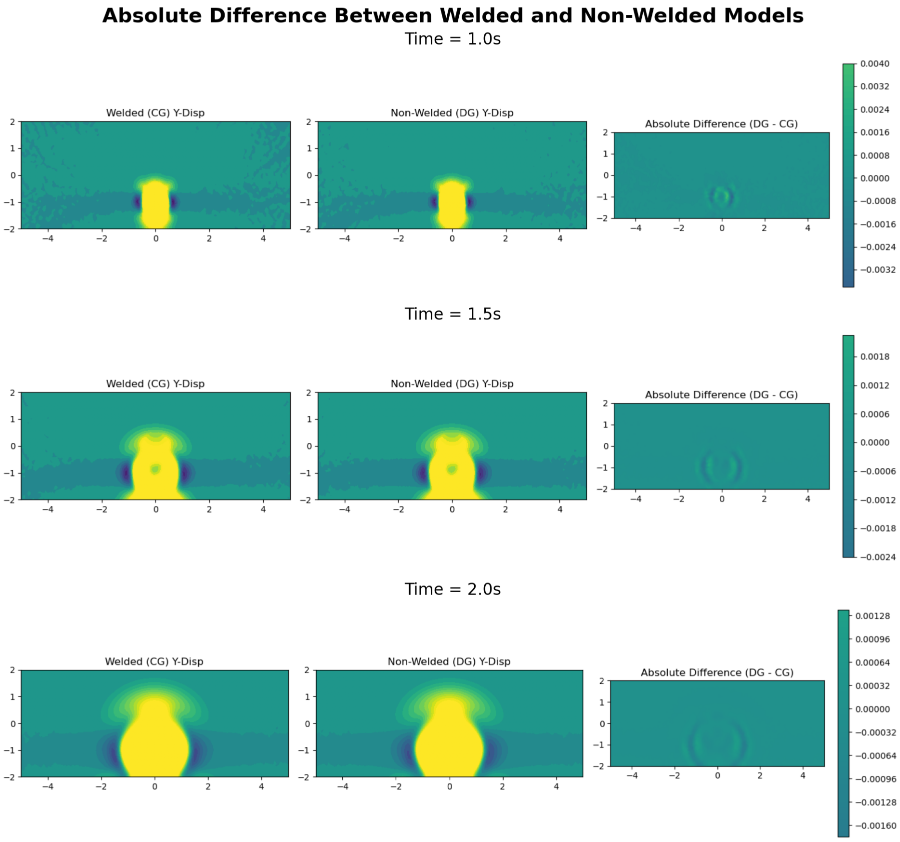

Figure 3: Absolute difference $|u_{\text{DG}} - u_{\text{CG}}|$ between welded and non-welded elastic wavefields. The discrepancy originates at the inclusion interface and propagates outward.

4.2 Inversion convergence: CG vs. DG

Figure 4 presents the key result of the cross-test. The CG solver (red) achieves a numerically lower misfit (7.3×10^{-6} at iteration 12) compared to the DG solver (1.6×10^{-5}). However, this apparent superiority is misleading: the CG solver cannot represent the interfacial slip physics in the data and compensates by biasing the density parameter.

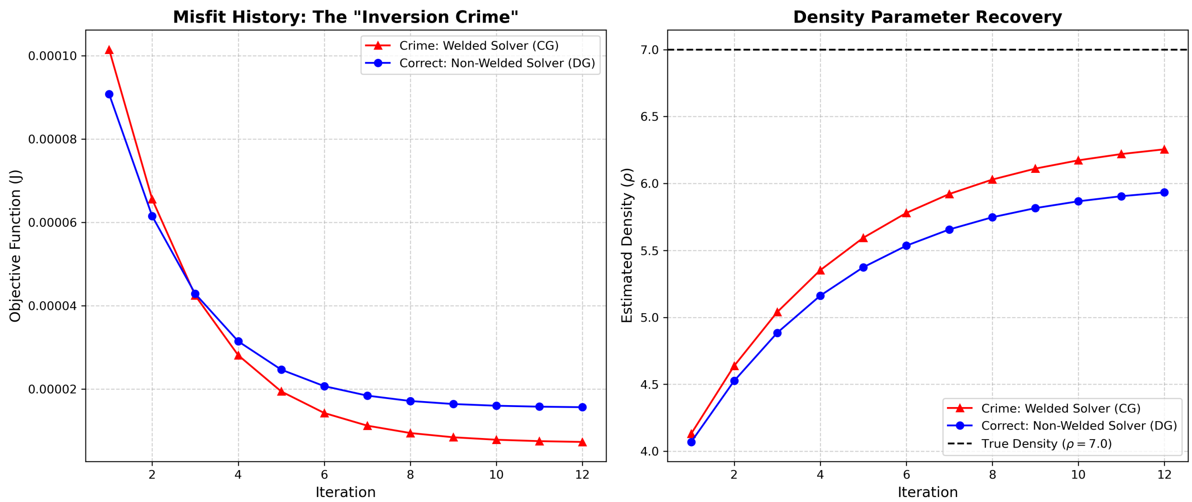

Figure 4: Cross-test results. Left: objective function history. Right: density recovery. The CG solver (red, welded) achieves lower misfit by absorbing slip physics through biased density; the DG solver (blue, non-welded) maintains physical consistency. Dashed line: true density $\rho = 7.0$.

The density recovery trajectory (right panel, Fig. 4) quantifies this bias. At iteration 12:

- CG solver: $\rho = 6.26$ (89% of the true value 7.0)
- DG solver: $\rho = 5.93$ (85% of the true value 7.0)

The CG solver recovers a higher density than the DG solver, not because it better resolves the inclusion, but because the inflated density absorbs wavefield energy attributable to interfacial slip. The CG "solution" is physically inconsistent: the recovered $\rho = 6.26$ does not represent the true material property but rather an effective parameter compensating for the missing slip mechanism.

4.3 Parameter convergence trajectories

Table 1 summarises parameter values at iterations 1, 6, and 12 for both solvers. The CG solver's density increases monotonically, while its shear modulus remains frozen at $\mu = 1.0$ — further evidence that the CG inversion attributes the slip-induced wavefield modification entirely to density rather than distributing the misfit across multiple parameters.

Table 1: Parameter recovery at selected iterations. True values: $\rho = 7.0$, $\mu = 2.0$, $\lambda = 4.0$.

Solver	Iter.	ρ	μ	λ	Misfit
CG (welded)	1	4.13	1.00	2.00	1.02×10^{-4}
	6	5.78	1.00	2.00	1.43×10^{-5}
	12	6.26	1.00	2.00	7.33×10^{-6}
DG (non-welded)	1	4.07	1.00	2.00	9.08×10^{-5}
	6	5.54	1.00	2.00	2.07×10^{-5}
	12	5.93	1.00	2.00	1.57×10^{-5}

5 Discussion

The cross-test results expose a fundamental limitation of CG-based FWI when the subsurface contains non-welded interfaces. The CG solver's inability to represent interfacial slip forces it to compensate through parameter bias, producing density estimates that are systematically higher than the DG solution. While the CG misfit is numerically lower, the physical interpretability of the recovered model is compromised.

This phenomenon is closely related to the concept of *inversion crime* in seismic tomography (Rawlinson & Sambridge, 2010), where using an incorrect forward operator leads to biased results that may appear well-resolved by formal metrics. Our results demonstrate that the "crime" is not merely a theoretical concern: it produces quantifiable parameter bias in a controlled synthetic experiment.

5.1 Implications for exploration seismology

In field applications, the true interfacial condition is generally unknown. Karst cavities, fractured rock masses, and masonry–soil contacts all represent environments where welded-boundary assumptions may be inappropriate. Our results suggest that CG-based FWI in such environments should be interpreted with caution: the recovered density may reflect an effective parameter that combines material contrast with unmodelled interfacial physics.

We do not advocate replacing CG solvers with DG solvers in all FWI applications. For welded geological interfaces — such as sedimentary layer boundaries with intact contacts — the CG formulation remains appropriate and computationally advantageous. Rather, our results highlight the importance of *model selection*: the choice of forward operator should be guided by prior knowledge of the interfacial conditions.

5.2 Computational considerations

The DG formulation increases the system size through additional interface degrees of freedom and requires a penalty parameter γ that balances accuracy and conditioning. In our implementation, the DG system is solved using the MUMPS direct solver, which handles the increased condition number robustly. For larger-scale problems, iterative solvers with appropriate preconditioners would be necessary.

The adjoint-free gradient computation using central finite differences requires $2N_m$ forward solves per iteration. For the three-parameter inversion ($N_m = 3$), this amounts to six solves per iteration — a manageable cost for the model sizes considered here but potentially prohibitive for 3D problems, where adjoint-based gradient computation would be preferred.

5.3 Limitations

Our study is limited to a two-dimensional, small-scale model with a single circular inclusion. The parameter recovery has not fully converged after 12 iterations, and both solvers have yet to reach the true density of 7.0. Future work should extend the analysis to: (i) full convergence studies with sufficient iterations, (ii) three-dimensional geometries, (iii) more complex inclusion shapes, and (iv) field data examples where interfacial conditions can be independently constrained.

6 Conclusions

We have demonstrated that the choice of interfacial continuity assumption in elastic FWI — CG (welded) versus DG (non-welded) — has a measurable impact on parameter accuracy when the subsurface contains non-welded interfaces. Using a synthetic cross-test on a 2D elastic inclusion model, we show that:

1. The CG solver absorbs interfacial slip physics through biased density estimates, achieving numerically lower misfit at the cost of physical accuracy.

2. The DG solver, formulated with Nitsche's interior penalty method, maintains physical consistency and recovers more accurate parameter values.
3. The "inversion crime" — using a physically inconsistent forward operator — produces quantifiable parameter bias even in a controlled synthetic setting.

These results have practical implications for FWI applications in engineering geophysics, where non-welded interfaces are common. We advocate for explicit consideration of interfacial conditions in FWI model design and recommend DG-based formulations as a tool for quantifying the sensitivity of inversion results to these assumptions.

Acknowledgements

The author thanks the developers of the FEniCS project for providing an open-source platform that made this work possible. The author has no funding to declare and no conflicts of interest.

Data Availability

The code and data used to generate the results presented in this manuscript are available from the author's public repository at `https://github.com/ogiannopoulou` (project `p1_cavity`) and from the author upon reasonable request. The synthetic models, solver configurations, and convergence histories are provided there to enable reproduction of the cross-test experiments.

References

Ainsworth, M., 2006. Discontinuous Galerkin finite element methods for acoustic wave propagation problems, in: Contemporary Mathematics, American Mathematical Society, pp. 39–58.

Arnold, D.N., Brezzi, F., Cockburn, B. & Marini, L.D., 2002. Unified analysis of discontinuous Galerkin methods for elliptic problems, SIAM Journal on Numerical Analysis, 39(5), 1749–1779.

Fezoui, L. & Christon, M., 2005. High-order discontinuous Galerkin methods for computational acoustics and aeroacoustics, International Journal of Computational Fluid Dynamics, 19(4), 285–300.

Hansbo, A. & Hansbo, P., 2002. An unfitted finite element method, based on Nitsche's method, for elliptic interface problems, Computer Methods in Applied Mechanics and Engineering, 191(47–48), 5537–5552.

Logg, A., Mardal, K.-A. & Wells, G.N., 2012. Automated Solution of Differential Equations by the Finite Element Method, Springer.

Mavko, G., Mukerji, T. & Dvorkin, J., 2009. The Rock Physics Handbook, 2nd edn, Cambridge University Press.

Nitsche, J.A., 1971. Über ein Verfahren zur Lösung der Dirichletschen Problems bei der Gleichung $\Delta u = 0$, Archive for Rational Mechanics and Analysis, 40, 312–331.

Operto, S., Virieux, J., Amestoy, P., et al., 2013. 3D finite-frequency full waveform inversion of a crustal thickness model, Geophysical Journal International, 195(2), 1000–1026.

Rawlinson, N. & Sambridge, M., 2010. Seismic tomography of complex tectonic systems, Surveys in Geophysics, 31(2), 197–221.

Signorini, A., 1940. Sopra alcune questioni di elastostatica, Atti della Accademia Nazionale dei Lincei, Rendiconti della Classe di Scienze Fisiche, Matematiche e Naturali, 2, 271–279.

Tarantola, A., 1984. Inversion of seismic reflection data in the acoustic approximation, Geophysics, 49(8), 1259–1266.

Virieux, J., 1986. P-SV wave propagation in heterogeneous media: velocity-stress finite-difference method, Geophysics, 51(4), 889–901.

Virieux, J. & Operto, S., 2009. An overview of full-waveform inversion in exploration geophysics, Geophysics, 74(6), WCC1–WCC26.